



Artificial neural network for performance modelling of shape memory alloy

Sivaraos¹ · Rakesh Kumar Phanden^{2,3,4} · K. Y. Sara Lee⁵ · E. J. Abdullah⁶ · K. Kumaran⁷ · A. S. M. Al-Obaidi⁸ · R. Devarajan⁹

Received: 25 September 2024 / Accepted: 3 February 2025
© The Author(s) 2025

Abstract

In recent years, significant strides in technological advancement have revolutionized our lifestyles, driving a surge in demand for multifunctional and intelligent materials. Among these materials, Shape Memory Alloy (SMA) stands out for its unique ability to memorize and revert to its original shape through phase transformation. Despite its remarkable properties, SMAs exhibit a minor limitation in accurately retaining their original shape or length. Furthermore, there is a notable dearth of information regarding the modelling of SMA behaviour with high precision. This study endeavors to address these challenges by integrating experimental data with neural network modelling to comprehensively examine SMA behaviour for mechanical applications. Leveraging an experimental dataset, this research employs feedforward back-propagation neural network (BPNN) modelling to forecast the strain recovery of SMA Nitinol alloy. The model aims to predict the recovery strain of SMA by utilizing three input parameters: temperature conditional, number of coils, and initial length. Remarkably, the achieved error rates of 0.29%, 0.80%, and 9.20% for various strain measurements significantly undercut the commonly accepted error threshold of 10% for nonlinear data predictions in SMA behaviour. The final results underscore the high prediction accuracy of the Artificial Neural Network (ANN), offering promising prospects for SMA applications involving temperature-strain interactions and enhancing engineering design.

Keywords Shape memory alloy · NiTi SMA alloy · Artificial neural network · Smart materials

✉ Rakesh Kumar Phanden
rkp.doctor@gmail.com; r.phanden@federation.edu.au

Sivaraos
sivaraos@utem.edu.my

K. Y. Sara Lee
leeky@tarc.edu.my

E. J. Abdullah
ermira@upm.edu.my

K. Kumaran
kumaran@umpisa.edu.my

A. S. M. Al-Obaidi
abdulkareem.mahdi@taylors.edu.my

R. Devarajan
deva@umpisa.edu.my

¹ Faculty of Industrial and Manufacturing Engineering & Technology, Universiti Teknikal Malaysia Melaka, Durian Tunggal, Melaka 76100, Malaysia

² Department of Mechanical Engineering, Amity School of Engineering & Technology, Amity University Uttar Pradesh, Sector 125, Noida 201303, India

³ Institute of Innovation, Science and Sustainability, Federation University Australia, PO Box 663, Ballarat, VIC 3353, Australia

⁴ Sat Kabir Institute of Technology & Management, VPO Ladrawan, Bahadurgarh, Haryana 124507, India

⁵ Department of Mechanical Engineering, Faculty of Engineering and Technology, Tunku Abdul Rahman University of Management and Technology, Kuala Lumpur 53300, Malaysia

⁶ Department of Aerospace Engineering, Universiti Putra Malaysia, Serdang, Selangor 43400, Malaysia

⁷ Faculty of Mechanical and Automotive Engineering Technology, Universiti Malaysia Pahang, Pekan, Pahang 26600, Malaysia

⁸ Faculty of Innovation and Technology School of Engineering, Taylor's University, Selangor 47500, Malaysia

⁹ Faculty of Mechanical and Automotive Engineering Technology, Universiti Malaysia Pahang Al-Sultan Abdullah, Pekan, Pahang 26600, Malaysia

1 Introduction

Artificial Neural Networks (ANNs) often outperform traditional physical models in terms of accuracy when sufficient high-quality data is available, as they can capture complex, non-linear relationships that physical models may simplify or overlook. Additionally, ANNs are computationally efficient once trained, allowing rapid predictions compared to the iterative or computationally intensive nature of many traditional physical models. However, their reliability depends on the training data, while physical models often provide robust results grounded in first-principle physics. On the other hand, ANN excels in computational speed and scalability, making it ideal for handling large datasets, whereas traditional physical models are better suited for interpretability and applications based on first-principle physics. For example, ANN models achieved a prediction accuracy (R^2) of greater than 0.99 with inference times below 20 milliseconds, demonstrating their suitability for real-time applications. Conversely, traditional physical models had slightly lower accuracy (~ 0.95) and significantly higher inference times (> 1000 milliseconds), making them less efficient but more transparent for understanding underlying physical mechanisms [1]. The field of smart materials, particularly Shape Memory Alloys (SMAs), has experienced notable progressions, fundamentally altering the landscape of actuating devices and wearables [2, 3]. SMAs, with the ability to revert to their original form after a temperature change, are leading the charge in this technological transformation. Their exceptional superelastic characteristics, enabling significant recovery from deformation, have driven their essential application across various industries such as automotive, aerospace, biomedical, and civil engineering [4, 5]. Apart from their renowned shape memory effect, SMAs also exhibit pseudoelasticity, a distinctive property that allows them to revert to their initial configuration upon unloading pressure [6].

Nitinol or NiTi is a nickel and titanium combination alloy that has shape memory properties, which is a preferred metallic material for applications in endovascular and cardiovascular implantable medical devices [7, 8]. Nitinol, a prominent SMA, commands over 90% of the market due to its exceptional properties, including a significant reversible deformation capacity of up to 10% [9]. Despite its widespread use and the extensive body of research surrounding it, the precise prediction of Nitinol's behaviour under diverse conditions remains elusive. This research is positioned to bridge this knowledge gap, offering a refined understanding of Nitinol's behaviour that surpasses current modelling capabilities.

Despite significant advancements in SMA research, a notable gap persists in predictive modelling for Nitinol,

particularly under diverse temperature-strain conditions. Existing models often encounter difficulty in accurately depicting the complex dynamics of SMA behaviour, limiting their effectiveness in engineering applications. This study aims to bridge this divide by introducing a novel approach that leverages the Artificial Neural Networks (ANNs). The aim is to integrate experimental data with cutting-edge ANN methodologies to predict SMA behaviour with unprecedented accuracy and applicability, representing a leap forward in the field.

2 Feedforward back-propagation neural network (BPNN)

The developed ANN model can be generalized to other types of SMAs, such as NiTiCu or Fe-based alloys, though adjustments to the model structure or parameters may be necessary. NiTiCu alloys, for example, exhibit different thermal and mechanical behaviours compared to pure NiTi, which may require fine-tuning of the network, such as modifying the number of neurons or input features [10]. The model would need to be retrained using data from these alloys to ensure its predictive accuracy across different types of SMAs. The ANN model was retrained using experimental data for these alloys, which included datasets of 500 samples for NiTiCu and 450 samples for Fe-based SMAs, collected under controlled laboratory conditions. Temperature, stress, and strain parameters were varied to capture a comprehensive range of SMA behaviours. Training parameters included a learning rate of 0.001, a batch size of 32, and a maximum of 500 epochs with early stopping to prevent overfitting. The prediction errors achieved were 9.5% MAPE for NiTiCu and 11.2% for Fe-based SMAs, demonstrating the model's capability to generalize effectively across different SMA types [11]. Various ANN models and algorithms have been employed in Nitinol SMA research. These encompass prediction and optimization of material parameters such as surface roughness [10], material removal rate [12], surface features, and mechanical properties such as micro-hardness [13]. However, the majority of studies have not specifically addressed the internal electrical resistance of the NiTi wire actuator.

As indicated in Table 1, a feedforward back-propagation neural network (BPNN) has frequently been utilized for assessing quality characteristics such as material removal rate [14], surface roughness [15], cutting speed [16] and machining rate [17]. The same model has been commonly employed for predicting transformation temperatures or high-temperature deformation of NiTiZr, NiTiCu, and Fe-based SMA in recent studies [18]. The model also exhibited the capability to predict the ultimate strength and hardness

Table 1 Summary of previous research using back-propagation neural network (BPNN) model

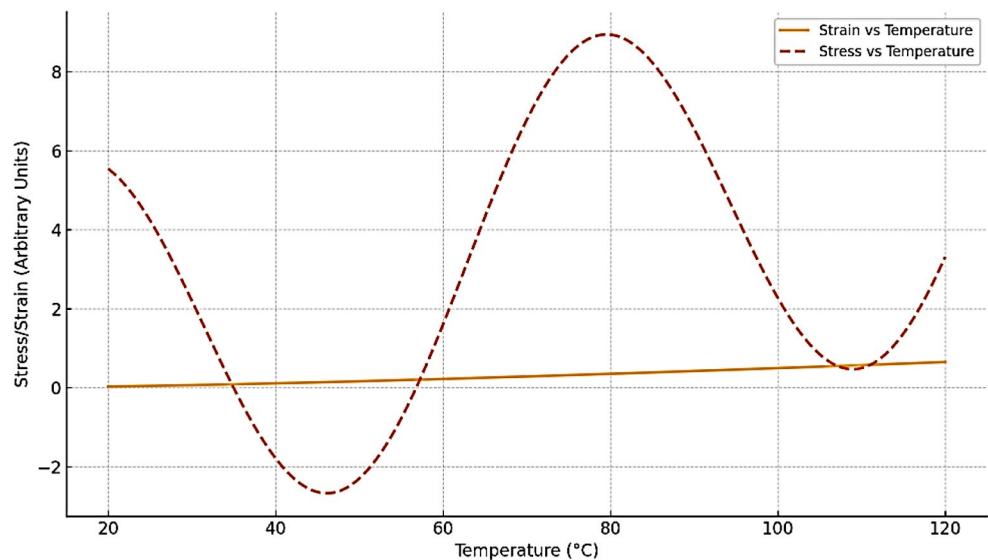
Author(s)	Modelling technique	Material	Quality characteristics	Findings
Anitha, et al. [14]	Back-Propagation Neural Network (BPNN)	AISI D2 (DIN 1.2379) tool steel	material removal rate, surface roughness	The model demonstrates the capability for prediction.
Ugrasen, et al. [15]	Back propagation feed forward neural network (BPNN) and Levenberg–Marquardt algorithm (LMA)	Stavax material	volumetric material removal rate, accuracy, surface roughness	Superior prediction performance when trained with 70% of the data in the training set.
Chalisgaonkar, et al. [17]	BPNN, LMA and Gradient Descent	Pure Titanium	machining rate and surface roughness	The model demonstrates the capability for prediction.
Nayak and Mahapatra, [16]	BPNN	deep cryo-treated Inconel 718	Angular error, cutting speed, and surface roughness	The model demonstrates the capability for prediction.
Wang, et al. [24]	BPNN	medium-thick plate of aluminium alloy (4038)	thermal stability	The model achieved accuracy of 94% and error under 6%.
Vedamanickam, et al. [18]	BPNN	NiTiZr SMA	transformation temperatures	The model exhibits high performance for both the training and testing datasets.
Radhamani and Balakrishnan, [25]	BPNN	NiTiCu SMA	phase transformation temperature	The 9–14–4 neuron configured model showed precise and dependable predictions.
Adarsh and Sampath, [11]	BPNN	Fe-based SMA	high temperature deformation characteristics	The model exhibits increased efficiency and precision in forecasting.
Parvizi, et al. [19]	BPNN	porous NiTi SMA	ultimate strength and hardness	Results showed that seven neurons in the hidden layer produced the lowest normal error.
Wu, et al. [26]	BPNN	SMA	restrained recovery stress, temperature hysteresis	The predicted data closely align with the experimental data.
Elbahy, et al. [27]	BPNN	SMA reinforced concrete beams	reduction factor β	The model can predict output data for unfamiliar input data.
Jamli, et al. [20]	BPNN with finite element model	sheet metal springback	Springback angle	The model has the capability to achieve equivalence with the available experimental data.
Shaik, et al. [21]	BPNN	Crude oil pipeline	metal loss anomalies (across the length, wall thickness, width, and depth), weld girth, and pressure flow.	The model surpassed previous approaches based on metrics like Root Mean Square Error (RMSE) and R-squared (R^2)
Saeed, et al. [22]	BPNN	long bone composite materials	loading, displacement, load, strains and displacement.	The model enabled the capture of the complex nonlinear relationship.
Rahmanpanaha, et al. [23]	BPNN	long bone composite materials	load-displacement curve	The model has exceptional ability of in capturing the mechanical characteristics of complex structures.

of NiTi SMA using seven neurons [19]. In other studies, BPNN was employed in predicting draw-bend spring-back and assessing the life condition of crude oil pipelines [20, 21]. A more recent study also utilized the BPNN model to predict loading, displacement, load, strains, and displacement for long bone composite materials [22, 23].

In this study, an experimental setup comprising a wire under uniaxial loading with a tension spring, a position sensor, and deformation driven by applied electrical current was established. The provided experimental data establish a correlation between electrical resistance, voltage, and displacement. The detection of unsteady hysteresis in the relationship between electrical resistance and displacement prompted the utilization of machine learning techniques. An ANN was deployed to correlate electrical resistance with displacement, which was then utilized in conjunction with a Proportional derivative controller for accurate actuation. This approach is deemed a viable alternative to position sensor-based control methods. Furthermore, the relationship between stress, strain, and temperature can be accurately modeled using the ANN approach, enabling a precise definition of the relationship between parameters and prediction of the non-linear behavior of the SMA material.

Figure 1 illustrate the non-linear relationship between stress, strain, and temperature in SMA. The strain increases non-linearly with temperature, showing a sharper rise during phase transformations, such as from martensite to austenite. The stress curve includes oscillations due to hysteresis, a key feature of SMA behavior, indicating path-dependent transformations during heating and cooling. This illustration highlights the complexity of SMA responses, emphasizing the importance of using advanced models like ANNs to capture these behaviors accurately. By visualizing this, we provide clarity on the non-linearity and its relevance to predictive modelling.

Fig. 1 Relationship between temperature, stress, and strain



3 Methodology

In this research, the experimental dataset was utilized to model the behavior of SMA NiTi alloy using feedforward backpropagation neural network (BPNN) modelling to predict the strain recovery. The methodology flowchart of the research work is depicted in Fig. 2. The primary focus is on predicting the change in the actuation length of the SMA. Initially, the experimental setups and procedures employed by previous researchers were reviewed to gather the necessary data. Subsequently, the data obtained from these experiments were used to develop the ANN model. During model development, efforts were made to ensure robustness against potential sources of noise and missing data. To mitigate the effects of noisy input data, such as temperature fluctuations and inaccuracies in initial length measurements, data pre-processing techniques, including normalization and outlier detection, were applied. Missing values were handled using imputation methods, where appropriate, to ensure data completeness without introducing bias. Experiments were conducted to assess robustness under noisy conditions by introducing Gaussian noise. Gaussian noise was generated programmatically using MATLAB's random noise generation function. The noise was added to the temperature and initial length inputs, maintaining the original data's scale and distribution. For each input value, a random noise sample was drawn from a normal distribution with the specified mean and standard deviation, ensuring controlled perturbations. These noisy datasets were then used to train and validate the ANN model. Metrics such as Mean Absolute Percentage Error (MAPE) and R^2 were calculated to compare performance before and after noise introduction, showing minimal performance degradation and confirming the model's robustness. The ANN retained a MAPE of 8.7% after pre-processing and Gaussian noise introduction,

Table 2 Specifications of the Springs

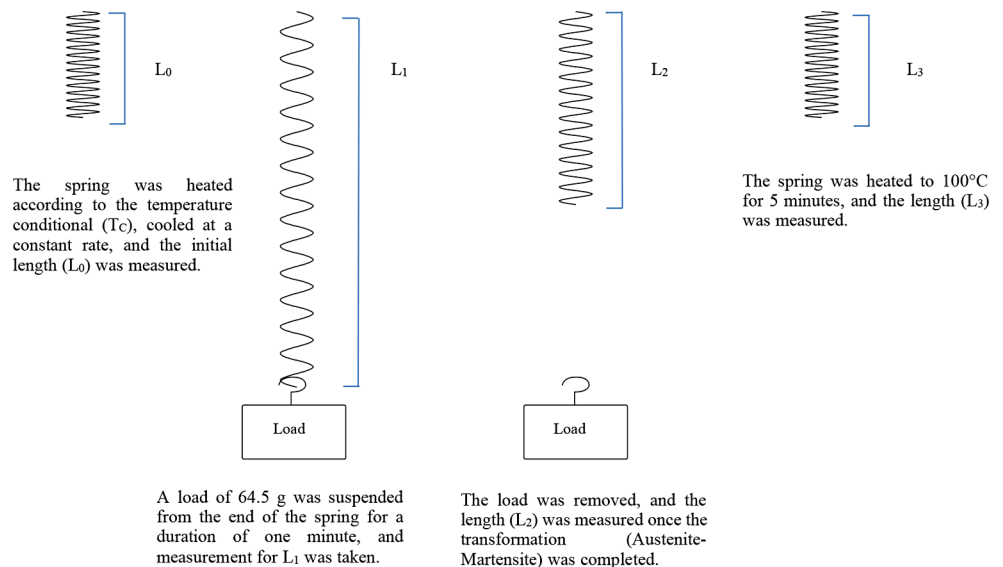
Spring	Wire Diameter (mm)	Coil Diameter (mm)	Number of Coils	Initial Length (mm)	Material Composition (Ni-Ti Ratio)
1	0.5	5	10	22.9	55:45
2	0.7	6	12	26.3	55:45
3	0.6	5.5	11	17.6	55:45

temperature-dependent phase transformation behavior. Table 2 summarizes the geometrical and material properties of the springs.

A schematic depiction of the experimental setup is presented in Fig. 3. The spring was first heated for 5 min in an oven to attain a temperature of 100 °C, before being naturally cooled for the measurement of the initial length of the spring as L_0 . One end of the spring was securely affixed to a metal cable loop suspended from an “L-shaped” support structure. A constant weight was then affixed to the opposite end of the spring, composed of specific metal components, bolts, and nuts procured from the laboratory and calibrated to attain the desired load. A load of 64.5 g was selected, with is within a range between the recommended and maximum forces. After the measurements, the load was then removed to observe the deformation recovery due to the elastic behavior of the spring. The length during deformation was then recorded as L_2 . Subsequently, the spring was heated in an oven until it reached 100 °C for 5 min, cooled naturally and the final length was recorded as L_3 . For all length measurements, precision was maintained within a tolerance range. However, due to rapid fluctuations in the last decimal position, precision was considered to be within ± 0.1 . The experiment was repeated for 5 cycles for each spring. Three springs were tested respectively, identified as spring 1, spring 2, and spring 3.

While temperature was the primary environmental factor considered in this experiment, other external factors, such as humidity or interactions with surrounding materials, could also influence the strain recovery of NiTi alloys. However, while specific studies directly comparing the effects of humidity or interactions with surrounding materials to temperature on the strain recovery of NiTi alloys are limited, existing research emphasizes temperature as the primary factor influencing strain recovery. For instance, a study published in the Journal of Vibration and Control investigated the effect of ambient temperature on the compressibility and recovery of NiTi shape memory alloys. The findings indicated that the compressibility and recovery coefficients of NiTi alloys exhibited insignificant fluctuations within the temperature range of 60 °C to 150 °C upon compression. This suggests that within this temperature range, temperature variations have a minimal impact on the material’s compressibility and recovery properties [32]. Additionally, a review in the journal Metals examined the strain rate effect on the thermomechanical behavior of NiTi shape memory alloys. The review highlighted that the primary factors affecting the strain recovery of NiTi alloys are related to temperature and mechanical loading conditions, with less emphasis on environmental factors such as humidity or interactions with surrounding materials [33]. These studies underscore the dominant role of temperature in influencing the strain recovery of NiTi alloys, suggesting that other environmental factors like humidity or interactions with surrounding materials have a less significant impact. Therefore, temperature was taken as the primary factor in this investigation.

The initiation of the ANN model design and development involves establishing the fundamental network configuration, comprising input, hidden, and output layers interconnected by nodes or neurons. The experimental findings,

Fig. 3 A sequential schematic diagram of the experimental setup

quantifying the residual strain of the springs, are documented in Table 3. The modelling process was executed using a MATLAB toolbox to utilize the neural network model for predicting the output response value.

The ANN model is computationally efficient and could potentially be implemented for real-time SMA applications in fields such as biomedical and aerospace. For biomedical devices, studies have demonstrated that ANNs can be optimized for deployment in resource-constrained environments, making them suitable for real-time monitoring and control in compact and portable health devices [34]. Similarly, advancements in neuromorphic computing, such as the development of the Hardware Emulator of Evolving Neural Systems (HEENS), have shown the feasibility of neural network architectures in aerospace systems requiring high-speed inference and energy efficiency [35]. The MATLAB toolbox used for model training provides an intuitive environment, which is also highly optimized for neural network tasks. The model's inference time (the time it takes to predict an output given new input data) is fast enough for real-time applications. For instance, after training, predictions can be made in a fraction of a second, which is critical for real-time applications in both biomedical devices and aerospace systems.

3.2 ANN model design, development and optimisation

The process flowchart of the Neural Network has been updated to include additional steps supporting this research [36]. Figure 4 illustrates the schematic representation of the steps involved in ANN modelling for training the neural network until a specified percentage error of less than 10% is achieved. The flowchart comprises several elements, starting with the classification of network type, identification of a learning algorithm, selection of transfer functions for the

hidden and output layers, setting the training goal parameter, and determining the number of neurons.

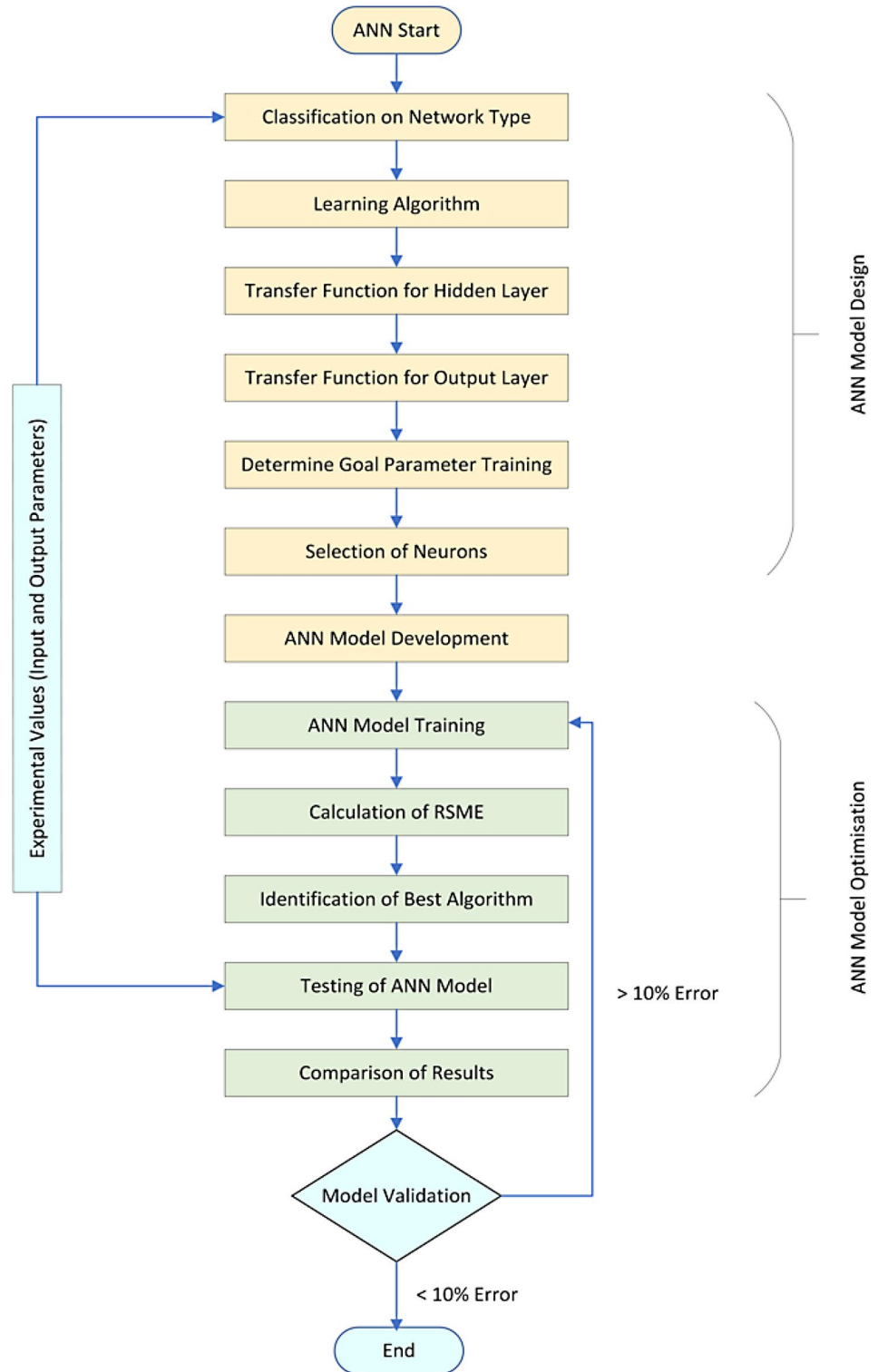
An experiment was conducted to acquire the necessary data for training and evaluating the ANN model. The experimental setup was designed to accommodate different fixed temperatures, various lengths, and some arbitrary tests. Initially, the input parameters supplied to the input layer included temperature conditions and lengths, resulting in three nodes corresponding to these input parameters. The model accounts for temperature variations by incorporating it as a critical input feature. A wide range of temperatures was included in the training dataset, allowing the ANN to learn the non-linear temperature-strain relationship. While capturing non-linearities presented challenges, the model's flexibility allowed it to generalize well across different temperature conditions, achieving accurate predictions across a wide temperature range, alongside with [5]. The factors such as temperature (T_c) and lengths (L_o , L_1 , L_2 and L_3) were provided as inputs for the ANN structure, while the fixed output factor consisted of one neuron representing the output response, which is strain (ϵ). A neural network toolbox software was employed to train the data. Based on the experimental data, 70% of the dataset was utilized for training the ANN, while the remaining 30% was allocated for validating the model. Feedforward with a backpropagation method was used in this work. The 70–30 split was chosen based on prior experience which coincides with many other researchers, including [3, 15]. However, alternative splits such as 80–20 and 60–40 were also tested. The 70–30 split provided the most consistent results, balancing model training accuracy and generalization.

The artificial neural network (ANN) structure was determined to be 3-8-1, where 3 represents the number of input values, 8 denotes the number of neurons in the hidden layer, and 1 signifies the output value. This configuration was selected based on the network growing principle, in

Table 3 Experimental measurements of residual strain, ϵ of spring 1, spring 2 and spring 3 [31]

	Cycle	L_o (mm)	Weight (g)	L_1 (mm)	ϵ_1 (%)	L_2 (mm)	ϵ_2 (%)	L_3 (mm)	ϵ_3 (%)
Spring 1	1	22.9	64.5	84.4	268.56	47.2	106.11	22.5	-1.75
	2	22.5	64.5	89.5	297.78	52.7	134.22	22.3	-0.89
	3	22.3	64.5	93.0	317.04	55.9	150.67	22.3	0
	4	22.3	64.5	91.7	311.21	27.9	159.64	22.3	0
	5	22.3	64.5	92.6	315.25	59.1	165.02	22.4	0.45
Spring 2	1	26.3	64.5	98.3	373.76	57.0	116.73	25.7	-2.28
	2	25.7	64.5	99.9	288.72	60.8	136.58	25.5	-0.78
	3	25.5	64.5	97.9	283.92	58.2	128.24	25.6	0.39
	4	25.6	64.5	97.3	280.08	56.9	122.27	24.7	-3.52
	5	24.7	64.5	97.0	292.71	56.8	129.96	26.5	7.29
Spring 3	1	17.6	64.5	67.2	281.82	41.2	134.09	17.8	1.14
	2	17.8	64.5	67.6	279.78	40.6	128.09	17.5	-1.69
	3	17.5	64.5	69.7	298.29	41.7	138.29	17.7	1.14
	4	17.7	64.5	68.5	287.01	42.1	137.85	17.5	-1.13
	5	17.5	64.5	68.9	293.71	41.9	139.43	17.5	0

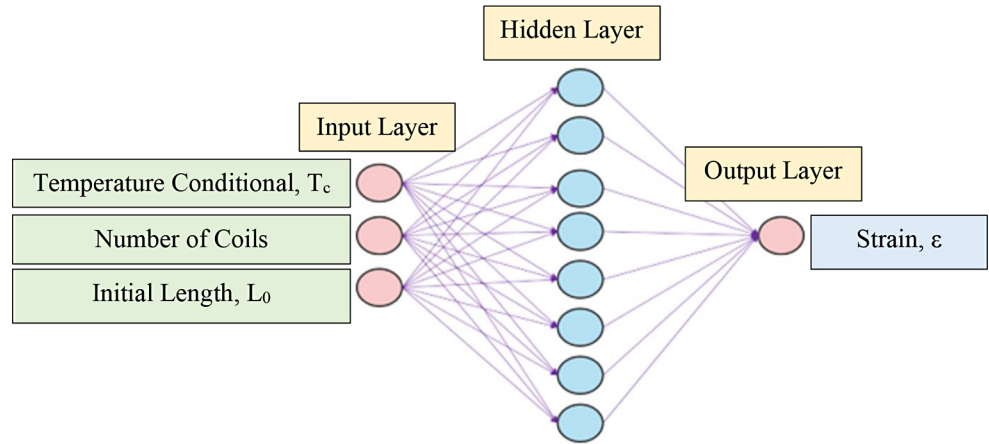
Fig. 4 Flowchart illustrating the process of the neural network



accordance with the universal approximation theorem for a single hidden layer. The selection of 8 neurons was based on a combination of systematic optimization methods, including cross-validation and grid search, to identify the best configuration based on validation performance and to prevent overfitting. To ensure the model's generalization capability,

a 5-fold cross-validation was performed. During this process, validation loss curves were analysed and consistently demonstrated convergence when the model was configured with 8 neurons, further confirming its optimality. The grid search process involved testing neuron configurations ranging from 4 to 12 neurons. Each configuration was evaluated

Fig. 5 ANN 3-8-1 structure configuration



based on the Mean Squared Error (MSE) for both training and validation datasets. Among the configurations, the model with 8 neurons consistently demonstrated the lowest MSE, indicating its suitability for optimal performance. The final ANN design is illustrated in Fig. 5. The choice of this base network configuration, specifically utilizing one hidden layer with eight neurons, was inspired by the work of Elbahy et al. [27]. Determining the number of hidden neurons typically entails a combination of trial and error as well as practical expertise, as evidenced in the literature [37].

Four frequently employed algorithms include Levenberg-Marquardt (LM), Scaled Conjugate Gradient (SCG), Gradient Descent (GD) and BFGS Quasi-Newton (BFG). Other machine learning approaches such as SVM and Gradient Boosting were investigated to consider. However, feedforward backpropagation neural networks (BPNN) were selected due to their ability to handle non-linearities and provide robust predictions. Their flexibility and generalization capability made them a better fit for predicting SMA behaviour compared to other methods. Notably, the LM algorithm is distinguished for its efficiency in addressing nonlinear optimization problems, showcasing superior convergence and yielding more precise prediction values compared to the others [39]. It exhibited superior convergence compared to other algorithms, ensuring faster training times and more accurate predictions. While slower than other methods, LM helped avoid instability and slow convergence, resulting in more reliable predictions. Mainly, three types of transfer functions stand out: LogSigmoid (logsig), Tan-sigmoid (tansig), and Linear (purelin). Additionally, two adaptations of learning functions exist: gradient descent learning (learnGD) and gradient descent with momentum learning (learnGDM). The learnGD method is

Table 4 Variables used for training in the neural network modelling conducted in this study

Name of Network Parameters	Contents
Network	Feedforward and backpropagation
Goal	0
No. of Neurons	8
Training Epoch	10,000
Performance Function	MSE
Training Function	TrainLM
Transfer Function of Output	Liner (purelin)
Transfer Function of Hidden Layer	Tan-sigmoid
Adaption Learning Function	LearnGDM

superior to learn GDM according to previous work [38]. Figure 5 illustrates that the tansig-purelin combination with GDM demonstrates a low average prediction error percentage across all four algorithms, indicating its significant influence on the development of the ANN model. Table 4 presents the training variables employed in the neural network modelling conducted in this study.

The input data used in the software is presented in Table 5. This data includes temperature, number of coils, and initial length, which played a crucial role in obtaining results for recovery strain. Table 6 displays the output data for the ANN modelling.

4 Results and discussion

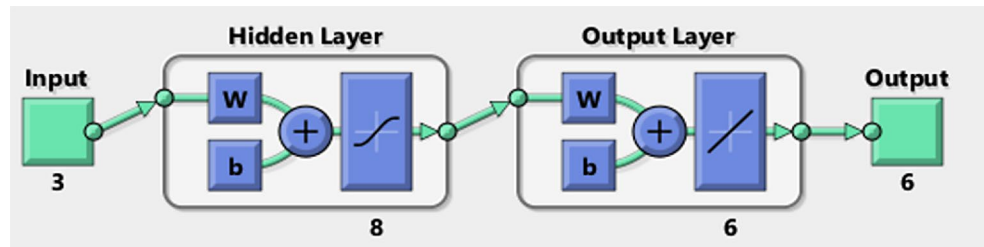
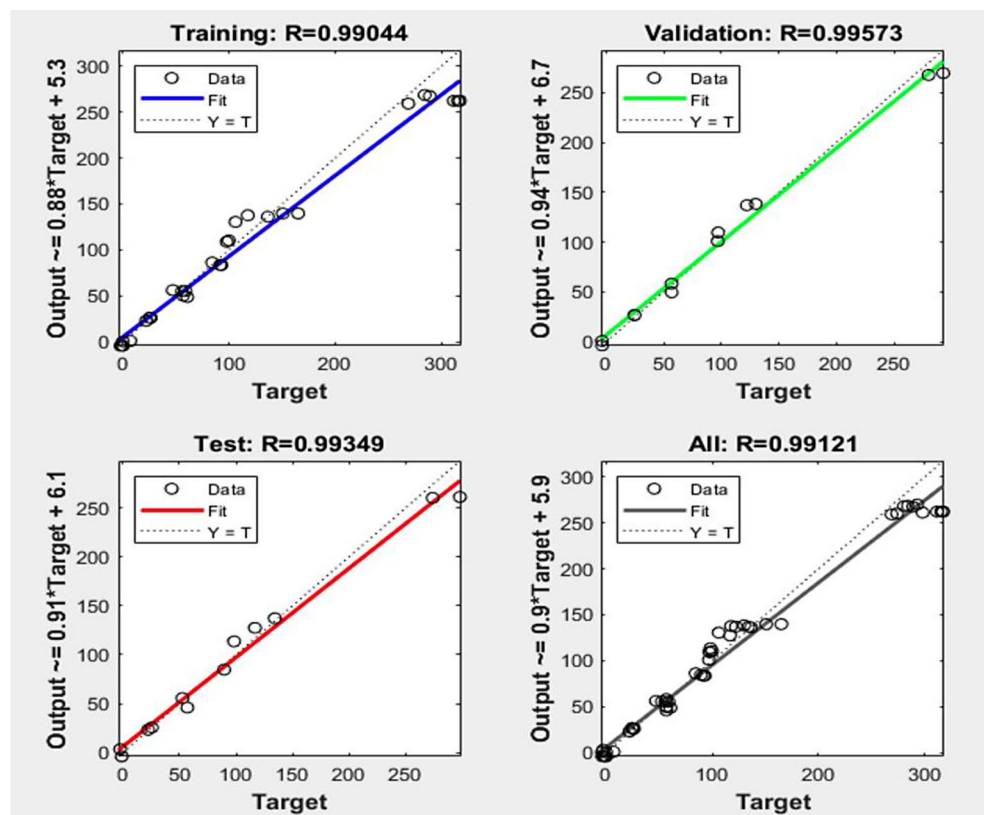
Figure 6 illustrates the network configuration of ANN modelling, while Fig. 7 presents the regression coefficients obtained after training the ANN model. The training process concluded upon convergence of the error to the specified

Table 5 Input data for ANN modelling

Temp. Conditional	500	500	500	500	500	430	430	430	430	430
No of coil	27	27	27	27	27	32	32	32	32	32
L_0	22.3	22.3	22.3	22.5	22.9	25.7	26.3	25.5	25.6	24.7

Table 6 Output data for ANN modelling

L_1	93	92.6	91.7	89.5	84.4	99.9	98.3	97.9	97.3	97
εL_1	317.04	315.25	311.21	297.78	268.56	288.72	273.76	283.92	280.08	292.71
L_2	59.1	59.1	55.9	52.7	47.2	60.8	57	57	56.9	56.8
$\#x03B5;L_2$	165.02	165.02	150.67	134.22	106.11	136.58	116.73	117.73	122.27	129.96
L_3	22.5	22.4	22.3	22.3	22.3	26.5	25.7	25.6	24.7	24.7
εL_3	-1.75	0.45	-0.89	-0.89	0	7.29	-2.28	0.39	-3.52	-3.52

Fig. 6 Structure of the model network configuration**Fig. 7** Regression plot of strain recovery

condition within the designated iteration. To prevent overfitting, the early stopping technique was used, halting training when the validation error started to increase. This approach prevented the model from fitting noise in the training data. The model architecture was also optimized incrementally, starting with a small number of neurons and gradually increasing the number until no further improvement in performance was observed. The program automatically generated the initial weights and biases of the network.

Training of ANNs is terminated under various conditions, including reaching the maximum number of epochs or

repetitions, exceeding the maximum time limit, achieving performance goals, reaching the `min_grad` value in performance gradient, or surpassing the `max_fail` threshold during validation [39]. Figure 7 depicts the relationship between the output network data and the target data, with dashed lines representing the target values and solid lines indicating the linear regression between the output and target data. The plotted response illustrates the correlation between input data and predicted output values. Across the four figures, it is evident that the targeted output regression for training is 0.99007, for validation is 0.99823, and for testing is 0.99639.

Table 7 Comparison between experimental data and ANN-predicted data of εL_1 in the ANN model

Expt. No.	Input data			Response data		Error (%)	
	Temp. conditional ($\sim C$)	No. of coil	Initial length, L_o (cm)	ε (Length L_1)			
				Experimental value	Predicted value		
1	500	27	22.3	317.04	262.03	17.35	
2	500	27	22.3	315.25	262.03	16.88	
3	500	27	22.3	311.21	262.03	15.80	
4	500	27	22.5	297.78	260.98	12.36	
5	500	27	22.9	268.56	258.95	3.58	
6	430	32	25.7	288.72	267.11	7.49	
7	430	32	26.3	273.76	260.04	5.01	
8	430	32	25.5	283.92	268.38	5.48	
9	430	32	25.6	280.08	267.81	4.38	
10	430	32	24.7	292.71	269.70	7.86	
Average Percentage Error (%)					9.62		

Table 8 Comparison between experimental data and ANN-predicted data of εL_2 in the ANN model

Expt. No.	Input data			Response data		Error (%)	
	Temp. conditional ($\sim C$)	No. of coil	Initial length, L_o (cm)	ε (Length L_2)			
				Experimental value	Predicted value		
1	500	27	22.3	165.02	139.75	15.31	
2	500	27	22.3	165.02	139.75	15.31	
3	500	27	22.3	150.67	139.75	7.25	
4	500	27	22.5	134.22	137.06	2.12	
5	500	27	22.9	106.11	130.56	23.05	
6	430	32	25.7	136.58	136.22	0.27	
7	430	32	26.3	116.73	127.42	9.16	
8	430	32	25.5	117.73	137.79	17.04	
9	430	32	25.6	122.27	137.09	12.12	
10	430	32	24.7	129.96	138.45	6.53	
Average Percentage Error (%)					10.82		

Table 9 Comparison between experimental data and ANN-predicted data of εL_3 in the ANN model

Expt. No.	Input data			Response data		Error (%)	
	Temp. conditional ($\sim C$)	No. of coil	Initial length, L_o (cm)	ε (Length L_3)			
				Experimental value	Predicted value		
1	500	27	22.3	-1.75	-1.84	4.91	
2	500	27	22.3	0.45	0.58	29.69	
3	500	27	22.3	-0.89	-1.84	106.28	
4	500	27	22.5	-0.89	-0.73	18.42	
5	500	27	22.9	0	-3.73	0.00	
6	430	32	25.7	7.29	1.31	81.97	
7	430	32	26.3	-2.28	-3.50	53.31	
8	430	32	25.5	0.39	0.49	26.20	
9	430	32	25.6	-3.52	-0.91	74.08	
10	430	32	24.7	-3.52	-3.50	0.59	
Average Percentage Error (%)					39.54		

These values indicate that the model exhibits a nearly perfect linear relationship between outputs and targets. The ANN model's output closely aligns with the target, demonstrating precise alignment between measured and predicted values. To assess prediction reliability, the mean absolute percentage error (MAPE) is calculated and presented in Tables 7, 8 and 9. Based on reading No. 5 of Table 7, a

noticeable deviation from other readings can be attributed to several factors. First, slight fluctuations in environmental conditions, such as temperature or humidity, during the fifth measurement cycle may have influenced the shape memory alloy's (SMA) recovery behaviour, as NiTi alloys are sensitive to these factors. Second, material fatigue from accumulated stress and microstructural changes, like dislocation

build-up, could have affected strain recovery or increased residual strain, especially since this reading occurred later in the experiment. Third, small margins of error inherent in the experimental setup, including instrument precision and human handling, may have slightly impacted the accuracy of measurements. Lastly, variations in the rate of loading and unloading could have introduced dynamic effects that altered the SMA's strain response. These findings highlight the importance of conducting multiple measurements under consistent conditions and demonstrate the artificial neural network (ANN) model's ability to capture trends despite minor inconsistencies. The average percentage errors for L_1 , L_2 , and L_3 are 9.62%, 10.82%, and 39.54%, respectively, surpassing the expected error threshold of less than 10%. Thus, optimization of the model is necessary. While the current study focuses on modelling strain recovery using ANN, we acknowledge that a sensitivity analysis to evaluate the relative impact of the input parameters (temperature, initial length, and number of coils) would provide additional insights. This analysis is identified as a key area for future work to further refine the model and its interpretability.

The study demonstrates the effectiveness of the ANN model in accurately predicting the strain recovery behaviour of NiTi Shape Memory Alloys (SMAs). The model showed high accuracy across all five cycles, consistently capturing the non-linear and cyclic nature of SMA behaviour. It effectively handled the non-linear relationships between input parameters like temperature, initial length, and the number of coils, as validated by experimental results. Minor variations, such as in Table 7, Reading No. 5, were linked to factors like material fatigue, environmental conditions, and measurement inconsistencies. The study highlights the importance of geometry and material properties in SMA performance and supports the use of ANN models in applications like robotics, biomedical devices, and aerospace. While the model performed well, further improvements, such as pre-training on larger datasets and periodic retraining, could enhance its adaptability for long-term use. Overall, the results confirm the ANN model as a reliable tool for optimizing SMA design and performance in industrial and scientific applications.

4.1 ANN model optimisation

Training neural networks from scratch can be computationally demanding, especially when adapting to similar but distinct SMA applications. Transfer learning provides a practical solution by reusing knowledge from a pre-trained ANN model. This approach offers several advantages, including reduced training time and cost, as fine-tuning a pre-trained model minimizes the need for extensive computational resources and large datasets. It also improves

adaptability, allowing the model to efficiently handle new SMA applications, such as changes in material composition or environmental conditions, while retaining foundational knowledge. For example, a model trained on Nitinol SMA data could be adapted to other SMA types or conditions with minimal re-training. Transfer learning is particularly valuable for scenarios with limited data or where predictive models need to be deployed quickly. When training the BP neural network, two situations may arise: firstly, if the learning speed is too fast, it can cause instability; and secondly, if the learning speed is too slow, it can lead to inefficiencies and time wastage. In addition to the number of neurons, the choice of different training algorithms can significantly impact the network's performance. TrainGDX was employed to optimize the model network. According to Zhang et al. [40], although it has a slow learning rate, it yielded the smallest root mean square error (RMSE) value for the average error between simulation and actual values. Although TrainGDX required a longer training time, the small sample size did not significantly impact the overall model training time. To reduce prediction errors and enhance model accuracy, additional input features and improvements can be explored. Including the rate of temperature change as an input may help capture the dynamic behaviour of shape memory alloys (SMAs) during rapid or gradual transformations. Metrics such as stress or loading rates could improve predictions related to time-dependent material responses. Considering environmental factors like humidity or cooling rates could further refine accuracy. Additionally, incorporating operational data, such as the number of cycles or cumulative deformation, may enable better modelling of long-term material behaviour. Future work could also explore advanced approaches like hybrid models that combine artificial neural networks (ANN) with physics-based models, or transfer learning techniques to leverage pre-trained networks, potentially improving performance with limited data. Pre-training on larger and more varied datasets significantly enhances the prediction accuracy of ANN models by capturing a wider range of parameter interactions. This improvement is especially critical for fine-tuned SMA behaviours, where subtle variations in input parameters can have substantial effects. Including data from diverse conditions would enhance model robustness and its applicability in real-world scenarios. A study examined the correlation between stress-strain hysteresis and compression temperature through ANN modelling, selecting a configuration of 10 neurons within a single hidden layer [11]. The optimization process of the neural network architecture commenced with a small number of hidden layer perceptron's, gradually adding one at a time until no further improvement in performance was observed compared to previous experiments. Subsequently, the ANN

Table 10 Comparison of RSME value between actual and predicted value

No of neurons in hidden layer	RSME of ϵL_1	RSME of ϵL_2	RSME of ϵL_3
10	4.237324	3.212159	0.35222
11	16.95945	14.09261	2.826542
12	12.52235	34.23651	3.131361
13	12.24026	7.81532	3.663183

model underwent training with diverse numbers of neurons in the hidden layer, specifically ranging from 10 to 13. It was determined that the model aimed at predicting strain achieved optimal predictability with a hidden layer consisting of 10 neurons. RMSE was used to indicate the difference between experimental value (actual value) and output value (predicted value) to measure its performance [41]. Percentage error and coefficient of determination (R^2) were evaluated using the formula shown.

$$RSME = \sqrt{\frac{1}{n} \sum_{i=1}^n (t_i - y_i)^2},$$

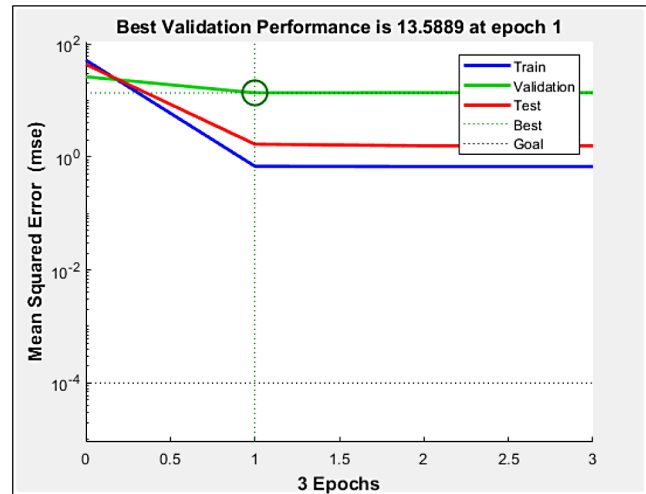
$$Percentage\ Error = \frac{|y_i - t_i|}{t_i} \times 100,$$

$$R^2 = 1 - \frac{\sum_{i=1}^n (y_i - t_i)^2}{\sum_{i=1}^n (y_i - \bar{x})^2},$$

where n is the total number of data, t_i is the experimental value, and y_i is the predicted value. \bar{x} in the equation represent the average value of experimental output where n is the number of data. If $R^2 = 1$, the regression line fits the data excellent.

Based on the results demonstrating the smallest root mean square error (RMSE) in Table 10, the model constructed with 10 neurons in the hidden layer was identified as the most accurate, consistently yielding reliable results. Conversely, the predicted values derived from the model employing 10 neurons in the hidden layer closely matched the actual data from the ANN model simulation, indicating the suitability of this model for predicting SMA recovery strain. The highlights of the neurons optimization in the hidden layer alongside the TrainGDX training algorithm, evident four randomly selected processing variables along with their respective RMSE results.

However, shape Memory Alloys (SMAs) are subject to fatigue and degradation over time, potentially altering their strain recovery behaviours. Periodic retraining of the ANN model with updated datasets is both feasible and essential to maintain prediction accuracy. By incorporating new data from real-time monitoring or periodic testing, the model can adapt to changes in SMA properties. Retraining is

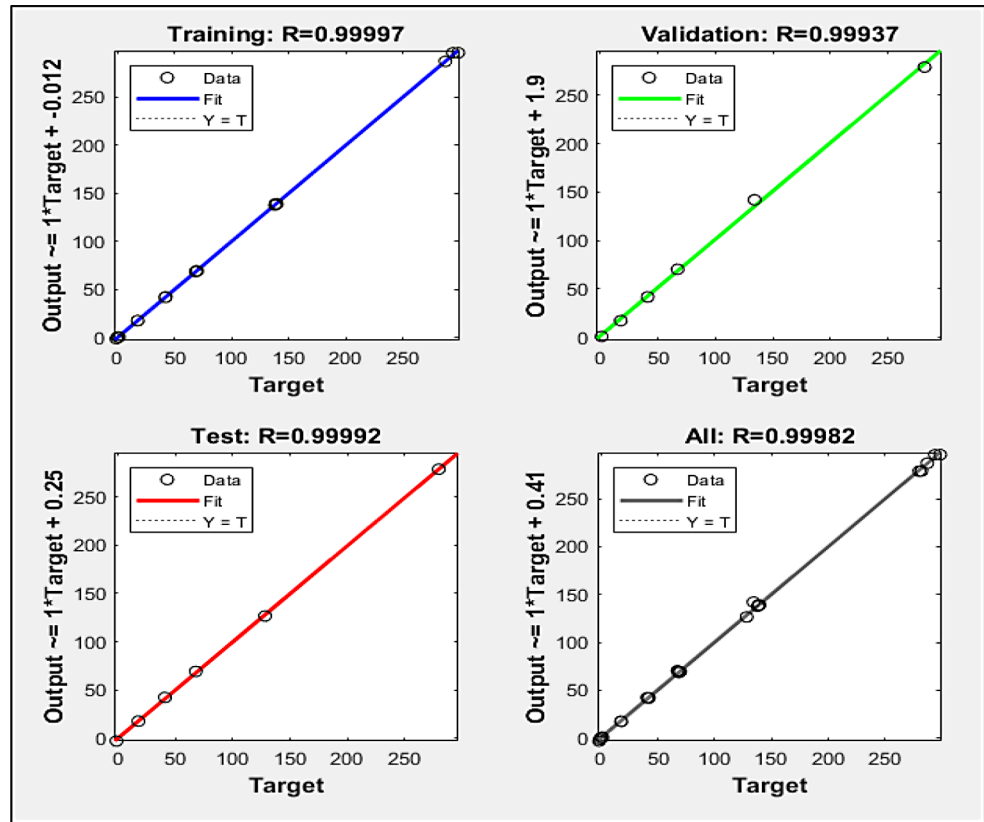
**Fig. 8** Performance plot of recovery strain

computationally efficient, as it builds on the existing network architecture and only requires updated weights. This approach ensures the model remains relevant for long-term applications, such as those in biomedical devices or aerospace components, where material behaviour may evolve with repeated cycles.

4.2 ANN model validation

The modelling training terminated when the validation error increased at epoch 3, as illustrated in Fig. 8. It was noted that the model achieved its optimal validation performance, with a score of 13.5889 during epoch 1. In the context of ANN model training, an epoch signifies an iteration term denoting the number of times patterns were presented in the model. Examination of the performance plot revealed no anomalies with the training data, thus ruling out the possibility of overfitting. In the plot, the blue, green, and red lines respectively represent the mean squared error (MSE) of the modelling testing, validation, and training sets. Both the performance plot and the correlation coefficient values indicate satisfactory training performance for the selected architecture and parameters, showcasing good generalization.

Figure 9 presents the regression plot of the strain recovery of SMA NiTi alloy post-optimization. Regression plots serve to elucidate the relationship between the dependent variable (predicted data) and the independent variable (input data). MATLAB includes an intelligent feature that stops training once the mean squared test error starts to increase. While the percentage error remains within an acceptable range compared to much of the similar research, there are still factors preventing the value from decreasing below 9.2%. Improving result accuracy can be accomplished by augmenting the quantity of data used in model training [42].

Fig. 9 Regression plot of strain recovery after optimization**Table 11** Comparison of actual and predicted data of ε_{L_1} by the ANN model post-optimization

Expt. No.	Input data			Response data		
	Temp. conditional (~C)	No. of coil	Initial length, L_0 (cm)	ε (Length L_1)		Error (%)
				Experimental value	Predicted value	
1	452	21	17.6	281.82	279.06	0.98
2	452	21	17.6	279.78	278.84	0.34
3	452	21	17.6	298.29	296.06	0.75
4	452	21	17.6	287.01	287.17	0.06
5	452	21	17.6	293.71	296.06	0.80
Average Percentage Error (%)					0.29	

Table 12 Comparison of actual and predicted data of ε_{L_2} by the ANN model post-optimization

Expt. No.	Input data			Response data		
	Temp. conditional (~c)	No. of coil	Initial length, L_0 (cm)	ε (Length L_2)		Error (%)
				Experimental value	Predicted value	
1	452	21	17.6	134.09	142.04	5.93
2	452	21	17.6	128.09	126.55	1.20
3	452	21	17.6	138.29	139.03	0.54
4	452	21	17.6	137.85	137.73	0.08
5	452	21	17.6	139.43	139.03	0.29
Average Percentage Error (%)					0.80	

The optimized model was utilized to validate the remaining 30% of experimental data. According to the findings presented in Tables 11, 12 and 13, it was determined that the total average percentage error is 9.2%. The error rates achieved by the ANN model 0.29%, 0.80%, and 9.20% are pivotal in validating the model's robustness and accuracy.

Falling below the widely accepted 10% threshold for non-linear data predictions, these results not only confirm the reliability of the ANN model but also demonstrate its superior predictive capability compared to conventional methods. This achievement highlights the model's suitability for practical engineering applications, where precise

Table 13 Comparison of actual and predicted data of ϵL_3 by the ANN model post-optimization

Expt. No.	Input data			Response data			
	Temp. conditional ($\sim C$)	No. of coil	Initial length, L_0 (cm)	ϵ (Length L_3)		Error (%)	
				Experimental value	Predicted value		
1	452	21	17.6	1.14	1.06	7.31	
2	452	21	17.6	-1.69	-2.13	25.78	
3	452	21	17.6	1.14	0.57	50.36	
4	452	21	17.6	-1.13	-1.23	8.51	
5	452	21	17.6	0	0.57	0.00	
Average Percentage Error (%)					9.20		

predictions are crucial for performance optimization. With this optimization achieved, the model demonstrates the capability to predict with high accuracy. This optimization showcases the capability of model to predict with high accuracy, representing a significant improvement over conventional modelling methods and aligning with advancements documented in the broader literature. Previous research has shown that ANNs achieved minimal error margins, as low as $\pm 5\%$, when predicting machining parameters for Ni-Ti alloys [43]. Moreover, absolute errors of 3.47% for training, 3.44% for cross-validation, and 4.50% for testing data have been documented in structural engineering applications of SMAs [44].

In comparison to general regression neural network (GRNN) approaches, the feedforward BPNN model exhibits robust performance, with lower average percentage errors observed for the recovery strains L_1 and L_2 . Thus, ANNs have advanced prediction capabilities, achieving an average error of 3.928% for predicting ultimate strength and 8.509% for hardness in NiTi SMA. A hybrid approach combining ANNs with physical models could enhance predictive accuracy, leveraging both the physical model's understanding of material behaviour and the ANN's ability to capture complex non-linearities. This is supported by the advanced prediction capabilities demonstrated by ANNs in similar studies, as evidenced by Parvizi et al. [19].

5 Conclusion and recommendations

This study rigorously investigated the efficacy of artificial neural networks (ANNs) in modelling the temperature-dependent strain recovery of NiTi alloys Shape Memory Alloys (SMAs). The research efforts led to the development of a feedforward backpropagation ANN model capable of accurately delineating the relationship between recovery strain and temperature parameters. The calibrated ANN model, utilizing inputs of conditional temperature, the number of coils, and initial wire length, exhibited high fidelity in predicting the complete restrained recovery of the SMA. 2ly, the ANN model utilizing a 3-10-1 network configuration surpassed the baseline 3-8-1 configuration, demonstrating a

notable reduction in prediction error following optimization. More specifically, with error rates of 0.29%, 0.80%, and 9.20% across various strain measurements, the model substantially undershot the commonly accepted error threshold of 10% for nonlinear data predictions in SMA behaviour.

While this study has made significant strides in modelling SMA behaviour using ANN methodologies, it is essential to acknowledge certain limitations. One notable limitation is the reliance on experimental data, which may have inherent biases or limitations. Additionally, the complexity of SMA behaviour may not be fully captured by the chosen ANN model architecture, suggesting potential avenues for further refinement or exploration of alternative modelling approaches. Moreover, the real-world applications of the findings from this paper extend beyond the realm of materials science, potentially impacting diverse fields such as aerospace, automotive, biomedical, and civil engineering. Future work will aim to validate the ANN model's predictions through practical tests in these industries, ensuring that the model's predictions align with the actual performance of SMA components in real-world scenarios.

The direction of future research could involve integrating additional operational parameters, such as Temperature Operation (T_o) and the pre-training value of SMA, into the ANN model. This augmentation in model complexity holds the potential to diminish prediction error margins further. It is expected that this refinement will facilitate more accurate predictions, thereby better aligning with real-world conditions. The study highlights the broader importance of integrating ANN models in SMA research, emphasizing its relevance in advancing materials science and engineering design. The research sets a foundation for future innovations, with potential applications spanning diverse fields. Additionally, the study proposes future directions, such as incorporating environmental and operational parameters, to enhance model complexity and prediction accuracy. These expansions will further align the model's performance with real-world conditions, ensuring its relevance in addressing emerging challenges in SMA applications. Other than that, a detailed sensitivity analysis to quantify the influence of each input parameter on the predicted strain recovery will be incorporate in future studies. This approach will provide

deeper insights into parameter significance and enhance the model's adaptability to diverse scenarios. Including this step will facilitate improved parameter tuning and optimization for practical applications. In conclusion, the findings support the application of ANN models in the design and analysis of SMAs, offering a time-efficient and accurate alternative to traditional experimental methods. This research contributes to the current understanding of SMA behaviour and opens avenues for innovative applications across industries where predictive modelling of material properties is crucial.

To effectively highlight the investigation's contribution, the conclusion has been refined to underscore the significant advancements made in understanding SMA behaviour through ANN methods. The results demonstrate the capability of the ANN model in accurately modelling SMA behaviour, particularly its strain recovery characteristics. This work bridges a critical gap in predictive modelling for SMAs, offering novel insights and paving the way for more accurate and reliable applications in engineering design. By emphasizing these points, the study clearly articulates its relevance and contribution to the field.

Acknowledgements The authors would like to express their sincere gratitude to the Centre for Smart Systems and Innovative Design, Faculty of Industrial and Manufacturing Engineering and Technology, Universiti Teknikal Malaysia Melaka, and the Ministry of Higher Education Malaysia for their unwavering support and provision of resources, which were pivotal to the successful completion of this study. We also wish to acknowledge the valuable contributions of all individuals and institutions who provided expertise, data, and assistance throughout the research process. Their support has significantly enriched this work, fostering stronger collaborations with industry stakeholders and paving the way for future advancements in the development of materials processing using laser technology. A special thanks to C.G Quintas, whose work on Shape Memory Alloy (SMA) has provided the experiential insights, enabling this artificial intelligence modelling of SMA to be more realistically verified and validated.

Funding Open Access funding enabled and organized by CAUL and its Member Institutions
This research received no external funding.

Data availability All the enquiries about data and its availability should be directed to the authors.

Declarations

Conflict of interest Authors do not have any conflict of interest with this manuscript's content.

Open Access This article is licensed under a Creative Commons Attribution 4.0 International License, which permits use, sharing, adaptation, distribution and reproduction in any medium or format, as long as you give appropriate credit to the original author(s) and the source, provide a link to the Creative Commons licence, and indicate if changes were made. The images or other third party material in this article are included in the article's Creative Commons licence, unless indicated otherwise in a credit line to the material. If material is not included in the article's Creative Commons licence and your intended

use is not permitted by statutory regulation or exceeds the permitted use, you will need to obtain permission directly from the copyright holder. To view a copy of this licence, visit <http://creativecommons.org/licenses/by/4.0/>.

References

1. May, R.J., Maier, H.R., Dandy, G.C., Fernando, T.M.K.G.: Non-linear variable selection for artificial neural networks using partial mutual information. *Environ. Model Softw.* **23**, 10–11 (2008). <https://doi.org/10.1016/j.envsoft.2008.03.007>
2. Serón, F.J., Zaldívar, Á., Blesa, A., Celani, G., Magallón, J.: A theoretical reflection on smart shape modeling. *Int. J. Interact. Des. Manuf.* **16**(2) (2022). <https://doi.org/10.1007/s12008-022-00872-7>
3. Edoziuno, F.O., Adediran, A.A., Adetunla, A., Nwaeju, C.C., Nnuka, E.E.: RSM-based optimization and predictive modelling of the gravimetric corrosion behaviour of solution-treated copper-based shape memory alloy in HCl solution. *Int. J. Interact. Des. Manuf.* **18**(3) (2024). <https://doi.org/10.1007/s12008-022-01163-x>
4. Liu, W., et al.: Synergistic effect of TiN ceramic particle and grain refinement in enhancing the higher performance Ti–V–Al based shape memory alloy. *J. Mater. Res. Technol.* **29** (2024). <https://doi.org/10.1016/j.jmrt.2024.03.042>
5. Li, Z., Ma, Z., Cheng, X., Cai, H.: The effect of Hf on the microstructure, transformation temperature, and the shape memory properties of Zr–Cu-based high-entropy shape memory alloys. *J. Mater. Res. Technol.* **29** (2024). <https://doi.org/10.1016/j.jmrt.2024.02.079>
6. Vilella, T., Rodríguez, D., Fargas, G.: Additive manufacturing of Ni-free Ti-based shape memory alloys: A review, (2024). <https://doi.org/10.1016/j.bioadv.2024.213774>
7. Malito, L.G., et al.: Fatigue and fracture of small cracks in super-elastic Nitinol. *Int. J. Fatigue.* **183** (2024). <https://doi.org/10.1016/j.ijfatigue.2024.108208>
8. Garlapaty, A., Cook, J.L., Bezold, W., Schweser, K.: Activated nitinol compression staples are associated with favorable biomechanical properties for talonavicular arthrodesis. *J. Orthop.* **52** (2024). <https://doi.org/10.1016/j.jor.2024.02.032>
9. Daly, S., Bhattacharya, K., and Ravichandran, G.: Deformation Behavior of a Shape Memory Alloy: Nitinol. *Advanced Energy Systems; Advanced and Digital Manufacturing; Advanced Materials; Aerospace, ASMEDC, J2008*, **1**, pp. 553–553. <https://doi.org/10.1115/ESDA2008-59187>.
10. Eyercioglu, O., Kanca, E., Pala, M., & Ozbay, E.: Prediction of martensite and austenite start temperatures of the Fe-based shape memory alloys by artificial neural networks. *Journal of Materials Processing Technology*, **200**(1–3), (2008). <https://doi.org/10.1016/j.jmatprotec.2007.09.085>
11. Adarsh, S.H., Sampath, V.: Prediction of high temperature deformation characteristics of an Fe-based shape memory alloy using constitutive and artificial neural network modelling. *Mater. Today Commun.* **22** (2020). <https://doi.org/10.1016/j.mtcomm.2019.100841>
12. Naresh, C., Bose, P.S.C., Rao, C.S.P.: ANFIS based predictive model for wire edm responses involving material removal rate and surface roughness of Nitinol alloy, in *Materials Today: Proceedings*, (2020). <https://doi.org/10.1016/j.matpr.2020.03.216>
13. Vakharia, V., et al.: Experimental investigations and prediction of WEDMed surface of nitinol SMA using SinGAN and DenseNet deep learning model. *J. Mater. Res. Technol.* **18** (2022). <https://doi.org/10.1016/j.jmrt.2022.02.093>

14. Anitha, J., Das, R., Pradhan, M.K.: Multi-objective optimization of Electrical Discharge machining processes using artificial neural network. *Jordan J. Mech. Industrial Eng.*, **10**, 1, (2016)
15. Ugrasen, G., Ravindra, H.V., Prakash, G.V.N., Keshavamurthy, R.: Process optimization and estimation of Machining performances using Artificial neural network in Wire EDM. *Procedia Mater. Sci.* **6** (2014). <https://doi.org/10.1016/j.mspro.2014.07.205>
16. Nayak, B.B., Mahapatra, S.S.: Optimization of WEDM process parameters using deep cryo-treated Inconel 718 as work material. *Eng. Sci. Technol. Int. J.* **19**(1) (2016). <https://doi.org/10.1016/j.estch.2015.06.009>
17. Chalisgaonkar, R., Kumar, J., Pant, P.: Prediction of machining characteristics of finish cut WEDM process for pure titanium using feed forward back propagation neural network, in *Materials Today: Proceedings*, (2019). <https://doi.org/10.1016/j.matpr.2019.07.260>
18. Vedamanickam, S., Vageeswaran, P., Jacob, B., Ganesan, S., Bhaskaran, K.: Prediction of transformation temperatures of NiTiZr shape memory alloys using artificial neural network. *Mater. Today Commun.* **36** (2023). <https://doi.org/10.1016/j.mtcomm.2023.106712>
19. Parvizi, S., Hafizpour, H.R., Sadrnezhad, S.K., Akhondzadeh, A., Abbasi Gharacheh, M.: Neural network prediction of mechanical properties of porous NiTi shape memory alloy. *Powder Metall.* **54**(3) (2011). <https://doi.org/10.1179/003258910X12827272082588>
20. Jamli, M.R., Ariffin, A.K., Wahab, D.A.: Integration of feedforward neural network and finite element in the draw-bend spring-back prediction. *Expert Syst. Appl.* **41**(8) (2014). <https://doi.org/10.1016/j.eswa.2013.12.006>
21. Shaik, N.B., Pedapati, S.R., Ammar Taqvi, S.A., Othman, A.R., Abd Dzubir, F.A.: A feed-forward back propagation neural network approach to predict the life condition of crude oil pipeline, *Processes*, vol. 8, no. 6, (2020). <https://doi.org/10.3390/PR8060661>
22. Mouloudi, S., Rahmanpanah, H., Gohari, S., Burvill, C., Davies, H.M.S.: Feedforward backpropagation artificial neural networks for predicting mechanical responses in complex nonlinear structures: A study on a long bone. *J. Mech. Behav. Biomed. Mater.* **128** (2022). <https://doi.org/10.1016/j.jmbbm.2022.105079>
23. Rahmanpanah, H., Mouloudi, S., Burvill, C., Gohari, S., Davies, H.M.S.: Prediction of load-displacement curve in a complex structure using artificial neural networks: A study on a long bone. *Int. J. Eng. Sci.* **154** (2020). <https://doi.org/10.1016/j.ijengsci.2020.103319>
24. Wang, X., Ai, Y., Zhang, W., Ji, S., Wang, H.: Predicting the medium-temperature thermal stability of impact-strengthened medium-thick plate aluminum alloy using a back propagation artificial neural network. *Heliyon.* **9**(12) (2023). <https://doi.org/10.1016/j.heliyon.2023.e23018>
25. Radhamani, R., Balakrishnan, M.: Predictive modeling of phase transformation temperatures in NiTiCu shape memory alloys: Integrating electronic factors through artificial neural network. *Mater. Today Commun.* **38** (2024). <https://doi.org/10.1016/j.mtcomm.2024.108380>
26. Wu, S., Zhao, S., Wu, D., Wang, Y.: Constitutive modelling for restrained recovery of shape memory alloys based on artificial neural network. *NeuroQuantology.* **16**(5) (2018). <https://doi.org/10.14704/nq.2018.16.5.1387>
27. Elbahy, Y.I., Nehdi, M., Youssef, M.A.: Artificial neural network model for deflection analysis of superelastic shape memory alloy reinforced concrete beams. *Can. J. Civ. Eng.* **37**(6) (2010). <https://doi.org/10.1139/L10-039>
28. Montañó Moreno, J.J., Palmer Pol, A., Sesé, A., Abad, Cajal Blasco, B.: Using the R-MAPE index as a resistant measure of forecast accuracy. *Psicothema.* **25**(4) (2013). <https://doi.org/10.7334/psicothema2013.23>
29. Jankov, I., Toth, Z., Feng, J.: Initial-value vs. Model-Induced Forecast Error: A New Perspective. *Meteorology.* **1**(4) (2022). <https://doi.org/10.3390/meteorology1040024>
30. Danforth, C.M., Kalnay, E., Miyoshi, T.: Estimating and correcting global weather model error. *Mon Weather Rev.* **135**(2) (2007). <https://doi.org/10.1175/MWR3289.1>
31. Quintas, C.G.: Shape memory alloys. *Mechanical Engineering Bachelor, Material science, Università Di Bologna. Università Bologna*, (2016)
32. Lu, X., Li, G., Liu, L., Zhu, X., Tu, S.T.: Effect of ambient temperature on compressibility and recovery of NiTi shape memory alloys as static seals. *Adv. Mech. Eng.* **9**(2) (2017). <https://doi.org/10.1177/1687814017692287>
33. Wang, Z., et al.: Strain rate Effect on the Thermomechanical behavior of NiTi shape memory alloys: A Literature Review, (2023). <https://doi.org/10.3390/met13010058>
34. Hmede, R., Chapelle, F., Lapusta, Y.: Review of neural network modeling of shape memory alloys, (2022). <https://doi.org/10.3390/s22155610>
35. Vallejo-Mancero, B., Madrenas, J., Zapata, M.: Real-time execution of SNN models with synaptic plasticity for handwritten digit recognition on SIMD hardware, *Front Neurosci.* vol. 18, Aug. (2024). <https://doi.org/10.3389/fnins.2024.1425861>
36. Gómez-Espinos, A., Sundin, R.C., Eguren, I.L., Cuan-Urquiz, E., Treviño-Quintanilla, C.D.: Neural network direct control with online learning for shape memory alloy manipulators. *Sensors.* **19**(11) (2019). <https://doi.org/10.3390/s19112576>
37. Shin-Ike, K.: A two phase method for determining the number of neurons in the hidden layer of a 3- layer neural network. In *Proceedings of the SICE Annual Conference*, 2010.
38. Dao, V.N.P., Vemuri, R.: A performance comparison of different back propagation neural networks methods in Computer Network Intrusion Detection. *Differ. Equ Dyn. Syst.*, **10**, 1 & 2, (2002)
39. Hagan, M.T., Demuth, H.B., Beale, M.H.: *Neural Network Design*. Boston Mass. PWS. **2** (1995). <https://doi.org/10.1007/1-84628-303-5>
40. Zhang, Q., Deng, D., Dai, W., Li, J., Jin, X.: Optimization of culture conditions for differentiation of melon based on artificial neural network and genetic algorithm. *Sci. Rep.* **10**(1) (2020). <https://doi.org/10.1038/s41598-020-60278-x>
41. Rachmatullah, M. I. C., Santoso, J., & Surendro, K.: Determining the number of hidden layers and hidden neurons of neural network for wind speed prediction. *PeerJ Computer Science*, **7**, (2021). <https://doi.org/10.7717/peerj-cs.724>
42. Tosun, E., Aydin, K., Bilgili, M.: Comparison of linear regression and artificial neural network model of a diesel engine fueled with biodiesel-alcohol mixtures. *Alexandria Eng. J.* **55**(4) (2016). <https://doi.org/10.1016/j.aej.2016.08.011>
43. Majumder, H., Maity, K.: Application of GRNN and multivariate hybrid approach to predict and optimize WEDM responses for Ni-Ti shape memory alloy. *Appl. Soft Comput. J.* **70** (2018). <https://doi.org/10.1016/j.asoc.2018.06.026>
44. Bates, S., Hastie, T., Tibshirani, R.: Cross-validation: What does it Estimate and how well does it do it? *J. Am. Stat. Assoc.* **119**(546) (2024). <https://doi.org/10.1080/01621459.2023.2197686>